Analytica Chimica Acta 1017 (2018) 20–25

Contents lists available at ScienceDirect

Analytica Chimica Acta

journal homepage: www.elsevier.com/locate/aca

# Design considerations for reducing sample loss in microfluidic paper-based analytical devices

Michael P. Nguyen [a], Nathan A. Meredith [b], Sydney P. Kelly [a], Charles S. Henry [a, *]

[a] Department of Chemistry, Colorado State University, Fort Collins, CO 80523, United States
[b] Department of Chemistry, University of Central Arkansas, Conway, AR 72032, United States

## HIGHLIGHTS

- Sample retention modes in μPADs were determined and minimized.
- Analysis shows ≤50% of Ni(II) deposited reaches the detection zone.
- Simple design considerations can improve sensitivity and colorimetric signal by 28% and 78%, respectively.
- The developed approach can be utilized with other analytes and detection motifs.

## GRAPHICAL ABSTRACT

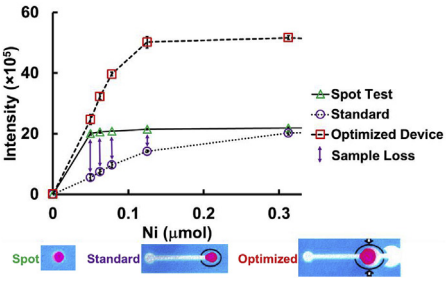


## ARTICLE INFO

*Article history:*
Received 20 September 2017
Received in revised form
18 January 2018
Accepted 19 January 2018
Available online 3 February 2018

*Keywords:*
Microfluidic paper-based analytical device (μPAD)
Sample loss
Colorimetric detection
Device fabrication
Wax printing

## ABSTRACT

The field of microfluidic paper-based analytical devices (μPADs) is most notably characterized by portable and low-cost analysis; however, struggles to achieve the high sensitivity and low detection limits needs required for many environmental applications hinder widespread adoption of this technology. Loss of analyte to the device material represents an important problem impacting sensitivity. Critically, we found that at least 50% of a Ni(II) sample is lost when being transported down a 30 mm paper channel that is representative of structures commonly found in μPADs. In this work, we report simple strategies such as adding a waste zone, enlarging the detection zone, and using an elution step to increase device performance. A μPAD combining the best performing functionalities led to a 78% increase in maximum signal and a 28% increase in sensitivity when transporting Ni(II) samples. Using the optimized μPAD also led to a 94% increase in maximum signal for Mn(II) samples showing these modifications can be applied more generally.



## 1. Introduction

Endeavors, such as the Human Exposome Project, demonstrate the growing interest in understanding the relationship between chronic exposure to environmental pollutants and changes in human health [1]. To understand complex exposures, efficient and selective methods are needed that can both identify and quantify chemical exposures from a variety of sources. Microfluidic paper-based analytical devices (μPADs) provide a tool that brings this level of analysis from the laboratory to the point-of-need due to their ease of use, portability, and low cost. Interest in μPADs has grown rapidly, and a number of applications have been developed in areas of both biological and environmental interest [2–9]. μPADs have used electrochemical and colorimetric detection motifs to measure concentration, with electrochemical detection frequently

* Corresponding author.
*E-mail address:* chuck.henry@colostate.edu (C.S. Henry).

https://doi.org/10.1016/j.aca.2018.01.036
0003-2670/

providing improved detection limits relative to colorimetric methods [10]. While the number and variety of applications continue to increase, an understanding of the paper properties that affect sensitivity has been lacking. Exploring the properties of paper as well as the interactions of samples and reagents with the cellulose substrate will enable further optimization of μPADs and related sensors.

Flow in μPADS is due to capillary action (imbibition) within the hydrophilic porous network; this flow may be modelled by Darcy's law and the Lucas-Washburn equation as described in multiple articles and reviews [11–13]. However, Li et al. identified a major limitation of current μPAD research as inefficient sample delivery to the detection zone through a combination of sample retention by the cellulose network and sample evaporation [14]. Due to sample losses during transport, limits of detection (LODs) on μPADs are frequently higher than traditional techniques or larger sample volumes are required to achieve comparable LODs. Recent work has focused on modifying flow rates and enhancing sample delivery by modifying the paper substrate using dissolvable bridges, creating flow channels with polymer films by applying coverings with varying contact angles, varying the channel geometries, or selecting substrates with different pore sizes [15–20]. While these studies have shown improvement, they have neither evaluated the fundamental impacts of the unmodified cellulose on sensitivity and detection limit nor provided simple solutions to aid in addressing this problem.

The work reported here expands on previous studies focusing on reducing sample retention within the cellulose network. To test strategies for reducing sample loss, colorimetric detection was chosen for its simple quantification. Using $Ni(dmg)_2$ as a model colorimetric system, sample retention in a lateral flow μPAD was indirectly determined by comparing the intensity of the detection zone against a spot test [21]. The spot test acts as a "zero-loss" test for which the sampling zone and detection zone are the same and there is no channel for sample loss. Sample loss to the cellulose was also determined by extracting the retained fraction into solution and quantifying with electronic absorption (UV-Vis) spectroscopy. The results suggested 50% or more of the initial sample never reached the detection zone. The extent of sample retention was investigated as a function of distance of travel, detection zone geometry, the inclusion of a flow-through waste region beyond the detection zone, fiber compression, and addition of a subsequent elution step. These investigations led to an optimized device, which resulted in a maximum signal increase of 78% and sensitivity increase of 28%.

## 2. Materials and methods

### 2.1. Materials

All of the following commercially available reagents were analytical grade and used as received without further purification: $NiSO_4 \cdot 6H_2O$, dimethylglyoxime (dmg), $MnCl_2 \cdot H_2O$, isopropanol, sodium tetraborate, and 4-(2-pyridylazo)resorcinol (PAR). The 0.1 M dmg solution was made using isopropanol. The $NiSO_4 \cdot 6H_2O$, $MnCl_2 \cdot H_2O$ and 0.1 M PAR solutions were made with Ultrapure water (18.2 MΩ cm) from a Mill-Q system (Merck Millipore Darmstadt, Germany) and used throughout. Whatman Grade 4 Qualitative (W4Qual) filter paper was purchased from GE Healthcare Life Sciences. Scotch™ heavy duty packing tape and 3 mil Scotch™ thermal lamination pouches sealed devices. The 0.1 M borate buffer was made using sodium tetraborate (pH 9.35).

### 2.2. Equipment

CorelDraw X4 was used for device design and the devices were printed on a Xerox ColorQube 8870 wax printer. A Xerox DocuMate 3220 was used to scan the devices prior to image analysis. ImageJ 1.49 was used to analyze the red colored $Ni(dmg)_2$ complex. An Agilent 8453 UV-visible spectrophotometer was used for electronic absorption measurements of $Ni(PAR)_2$ and $Mn(PAR)_2$. A Sartorius PR-50 pH meter with a PY-P28-2S electrode was used for all pH measurements and calibrated daily prior to use. A 30W $CO_2$ Epilog Laser Engraver was used to fabricate the wax-free devices. An Apache AL 13P thermal laminator was used to seal devices in lamination pouches.

### 2.3. Device designs

Devices were constructed by first cutting the Whatman paper into 8.5″ x 11″ sheets to fit them into the printer. A "Sky Blue" (R = 0, G = 124, B = 195) colored wax was used for the barriers to provide good contrast to the red-pink colored $Ni(dmg)_2$ complex. The diameter of the sample and detection zones for the standard device were 5 mm and the channel was 2.5 mm wide. From one end to another, the device was 30 mm long. These printed rings helped align the image analysis tool with a regular size and position. After devices were wax printed, the wax was melted (150 °C, 90s) into the fibers to create a hydrophobic barrier. An aluminum plate was placed over the device during heating to uniformly distribute pressure and heat. After melting, the bottom layer of the devices was sealed with Scotch™ Heavy Duty packing tape to prevent leaking. A 0.5 μL portion of borate buffer was first pipetted to the detection region and allowed to dry prior to adding 1 μL of the dmg ligand dissolved in isopropanol. Once the reagents were completely dry (~15 min), devices were ready for sample addition (Fig. S1). Laser cut, wax-free devices were also made for comparison. The dimensions of laser cut devices were the same as the melted wax devices. For laser cut devices, a filter paper sheet with packing tape on the back was used to create an array of devices that used only the edge of the device as a barrier. This method provided a leak-free barrier for the volumes used. All reagent depositions were identical to those for the wax devices. Laminated devices followed the same procedure as the other devices, but after the buffer and ligand deposition, the device was placed in a 3 mil thermal lamination sheet and melted with two passes into a laminator at 350 °F. Then the sampling zone was punched out with a hole-punch and resealed on the back with packing tape. To carry-out the extraction in Section 3.3, the detection zone was cut off a used device and the remainder of the device (sampling zone and channel) was placed in 4 mL of deionized water for 24 h to extract residual Ni(II). The resulting Ni(II) sample was analyzed by using PAR as the colorimetric indicator.

### 2.4. Image analysis

Image analysis was done using ImageJ following the procedure of Mentele et al. [22]. Instead of using the 8-bit grey scale, the green color space was used. This was achieved by splitting the color channels ("Image" → "Color" → "Split Channels") and using the "green" channel data. After the image was processed, the "oval" tool was used to select the image data for the detection zone area. In some devices, a circular black ring was added to the device to aid the oval placement and improve the consistency of the image analysis. The "Raw Integrated Density" values were divided by

$1 \times 10^5$ and used for the intensities in this work.

### 2.5. Data analysis procedure

To best quantify sample loss, units of moles were monitored versus signal intensity. When comparing the effectiveness of the various device designs, a comparison of the percent differences in maximum signal between 0 and 1.5 μmol Ni(II) were made. All reported values of maximum signal were statistically significant compared to the standard channel test as determined using a two-tailed sample T-test. The changes in sensitivity of each device were monitored by comparing the percent differences in the slopes of the intensities between 0 and 0.12 μmol Ni(II) (for 0, 0.05, 0.06, 0.07, 0.12 μmol). The percent differences in the slope were found to be statistically significant as determined from the error in the slope unless otherwise stated.

## 3. Results & discussion

### 3.1. "Zero-loss" and standard test

Most μPADs use channels to transport sample; however, the extent of sample loss due to transport is poorly understood. Sample loss to paper substrates is potentially complex; thus, the first test focused on understanding the amount of sample retention in the transport channel. A comparison of intensities for a zero-loss (spot test) and a standard (channel) device was evaluated for a 12.5 μL aliquot of nine Ni(II) concentrations (0–0.12 M). Images of the spot test and standard channel devices are shown in Fig. 1a. For consistency, the standard device had the same diameter detection zone as the spot test but incorporated a 30 mm long channel. The $Ni(dmg)_2$ intensity in the detection zones was analyzed 1 h after the Ni(II) sample was added. The spot test data (n = 6) showed a steep increase in signal with increasing Ni(II) concentration, reaching saturation near 1.3 times excess Ni(II) to dmg (the stoichiometric equivalence of $Ni(dmg)_2$ on Fig. 1a is located between values 0.078 & 0.125 μmol). The channel device data (n = 5) does not show saturation until 15 times excess of Ni(II) (Fig. 1a). The data suggests the channel is responsible for retaining >50% of the Ni(II) below 0.15 μmol. Next, we explored potential modes of sample retention (wax barrier, inlet, channel length, etc.) to understand and minimize sample loss.

### 3.2. Wax barrier

To direct flow, wax printed barriers are commonly used to create channel barriers [23]. Despite being hydrophobic, wax barriers are still porous and provide potential modes for sample retention. The wax barrier was investigated as a mechanism for retaining sample. When removing the wax barrier (laser cut devices, n = 4), there was a 20% decrease in maximum signal and a 15% decrease in sensitivity (Fig. 1a). The wax barrier thus improved sample delivery to the detection zone compared to laser cut devices. By contrast, the sample speed through the laser cut devices was noticeably faster when compared to their wax counterparts. Flow rate has previously been shown to decrease with the addition of wax barriers but also results in an increased signal intensity for colorimetric detection schemes [24]. With the differences in flow rate between wax printed and laser cut devices, the speed rather than the porous wax barriers appears to more significantly affect the device performance.

### 3.3. Channel retention

As observed in the spot test versus standard device, much of the sample is retained by the standard device. Having examined the effect of the paper channel on the intensity of the deposited sample, a test of how cellulose retained metals was of great interest. Cellulose has been reported to have a weak affinity for metals [25]. To test the strength of these Ni–cellulose interactions in a μPAD format, the detection zone of a used device was placed in 4 mL of deionized water to extract residual Ni(II). The resulting Ni(II) sample was analyzed using PAR as the colorimetric indicator. A plot of the theoretical amount of sample detected versus the actual amount of sample detected is shown in Fig. 1b. The values obtained from the UV-vis measurements reflect how much Ni(II) is lost to the device. Between 0 and 0.6 μmol, up to 50% of the sample does not reach the detection zone. Despite cellulose's β-D-glucose repeating units having low affinity (0–0.955 mmol metal·$g^{-1}$ cellulose) for metals, this study confirmed there is enough affinity between the cellulose network and the Ni(II) that sample is retained in the channel even after soaking in water overnight [25,26].

### 3.4. Water elution

When most analytes are added to μPADs for colorimetric detection, there is no ancillary treatment to increase the analyte transport, leaving significant analyte in the transport channel undetected, as shown in our previous tests. It has previously been reported that a washing step can help eliminate unbound antigen and antibody from μPADs [27]. Our next experiment evaluated the effectiveness of a similar elution step aimed to transport retained sample to the detection zone. To do this, a second elution of water was added to the sample inlet of the device after the original Ni(II) reached the detection zone and dried (~15 min). The $Ni(dmg)_2$ intensities were compared before and after washing (Fig. 1c). The

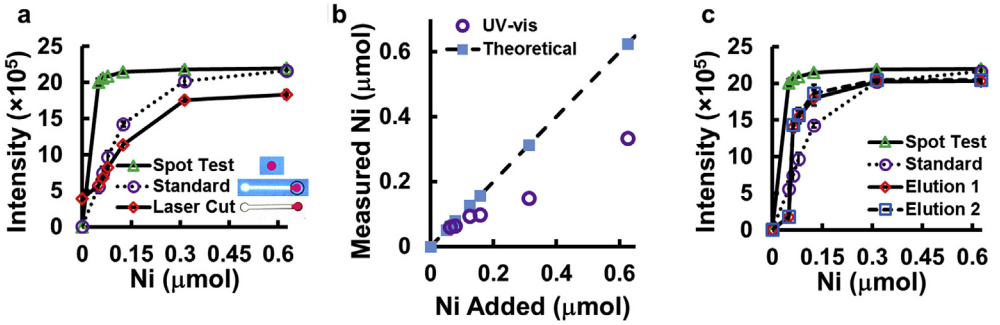


**Fig. 1. a.** Plot showing intensity of the spot test and the standard channel device versus the laser cut device. Images of these devices are placed in the plot for visualization (inset: devices are shown to right of the legend, respectively). **b.** The open circle data set shows the number of moles of Ni(II) detected through UV-vis. The closed diamond data set shows the actual amount of moles of Ni(II) deposited on the device. **c.** Comparison of the elution steps after a standard sampling.

washing method was effective at moving more sample to the detection zone, leading to an increase in sensitivity of 8% despite a decrease of 7% in the maximum signal (n = 5). Here the sensitivity difference with the washing step is not statistically significant; however, the step is efficient at increasing the sensitivity when combined with other modifications as seen in Section 3.10. A possible rationale for this increase in performance is that once the front of the solution front reaches the detection zone, there is no longer a driving force (or capillary action) to keep sample traveling toward the detection zone. There may be a slight increase of sample transport by diffusion when the whole channel is wet, however, due to evaporation, this effect is minimal at best.

### 3.5. Distance

Distance is believed to be an important consideration when designing devices due to issues of evaporation hindering sample transport and the ability of the cellulose network to retain the analyte. The distance between the detection and sampling zones was thusly studied. A device was fabricated where the distance between the detection and sampling zones was varied from 11 to 44 mm (Fig. 2a). The further the detection zone is from the sampling zone, the lower the Ni(II) intensity (n = 3) as shown in Fig. 2b, which is not surprising given prior results in Section 3.1.

### 3.6. Sampling zone

Based on initial results indicating retention of metals by the paper substrate, the impact of inlet geometry on signal was tested. The shape of the sampling zone was varied from the traditional circular zone to a simple rounded tip (small inlet) the width of the microfluidic channel (Fig. S3). When the circular inlet was replaced with the small inlet, the speed at which the sample flowed greatly increased, reducing overall assay time. The faster assay resulted in a decrease of maximum signal by 4% with no statistically significant change in sensitivity (n = 5). Despite the small decrease in signal as a result of the geometry change in the sample inlet, increasing the speed of the sample delivery successfully decreased total analysis time.

### 3.7. Detection zone

While it is likely much of the unmeasured Ni(II) remains in the channel, it is also possible that sample complexed by dmg under the paper surface is not detected. If true, then increasing the surface area of the detection zone would increase the measured intensity per μmol of Ni(II). To test this hypothesis, the detection zone area was increased two-fold, while the same volume and concentration of buffer and ligand added to the device. To fully cover the detection zone, dmg was deposited onto the device so that the edge of the reagent dried at the interface between the channel and the detection zone. By doubling the size of the detection zone, the maximum signal was increased by 63% and the sensitivity increased by 21% (Fig. 3a, n = 5). By far, this manipulation had the highest increase in both performance metrics. Some bleeding of the red colored complex outside of the distinct red circle was observed with the larger zone. Future experiments using thinner paper could address this problem. We suspect that with thinner paper, there would be more exposed surface area relative to the total volume, resulting a higher signal.

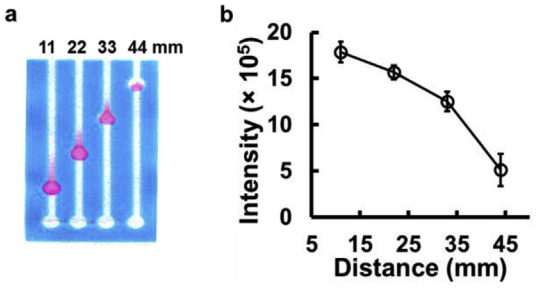


**Fig. 2. a.** Devices showing distance dependence of $Ni(dmg)_2$ signals. **b.** Plot showing the effect of distance on the sample intensity of $Ni(dmg)_2$ at 3.25 mM Ni(II).

### 3.8. Waste zone

In the distance dependence study, it was observed that some $Ni(dmg)_2$ complex passed out of the detection zone as there was no barrier stopping sample flow. This raised the question whether adding a "waste zone" at the end of the device would help increase sample wicking to the detection zone. It has been previously shown by Mendez et al. that incorporating a 270° hemisphere fan to the end of a microfluidic channel can be used to generate a constant flow rate once the sample reaches the fan [28,29]. Adding the fan increased the maximum signal by 15% and the sensitivity by 10% (Fig. 3b). There was a small amount of bleeding of the $Ni(dmg)_2$ complex in the channel past the detection zone; however, the complex is insoluble in water so this bleeding was not extensive.

### 3.9. Mechanical compression

Lastly, pre-swelling and lamination of the devices were explored. The pre-swelled devices were soaked in water and allowed to dry before use. The purpose for swelling the fibers was to create smaller channels and mimic conditions where devices are pre-wetted during fabrication or use. It is believed that lamination mechanically compresses the pores in addition to reducing evaporation. Through the pre-wetting step, the maximum signal is increased by 7% but the sensitivity difference was not statistically significant (n = 5). Lamination of the device increased signal by 29% but the sensitivity decreased by 7% (Fig. 3c, n = 5). Generally, the manipulations that exhibited higher maximum signals exhibited higher sensitivity values as well. However, for the pre-swelled and laminated devices, lower sensitivities and higher maximum signals were observed. Surface area measurements (BET analysis) of cellulose show that water can swell fibers by 61%, creating pores with smaller diameters [30]. This compression of the pores may also provide unique pathways for the fluid to travel as the swelling process irreversibly eliminates the cellulose supramolecular structure [31]. Mechanical energy associated with lamination can degrade the cellulose supramolecular structure by disrupting its fibrillar architecture [32]. This collapsing of the supramolecular structure in both manipulations ultimately leads us to conclude that a collapse the of the cellulose supramolecular structure causes the unique behavior. Fidale et al. has studied the effects of swelling of fibers in various aprotic and protic solvents to tune the substrate to exploit this phenomenon [33]. Further studies are underway to understand the specific factors associated with pre-wetting and laminating that impact sample delivery.

### 3.10. Additive device

Based on prior results, a device was fabricated combining the manipulations (small inlet, larger detection zone, waste zone and an elution step) that increased the sensitivity and maximum signal. This additive device resulted in an increase in signal and sensitivity of 73% and 23%, respectively for the resulting device. After the elution of water in this device, the maximum signal and sensitivity

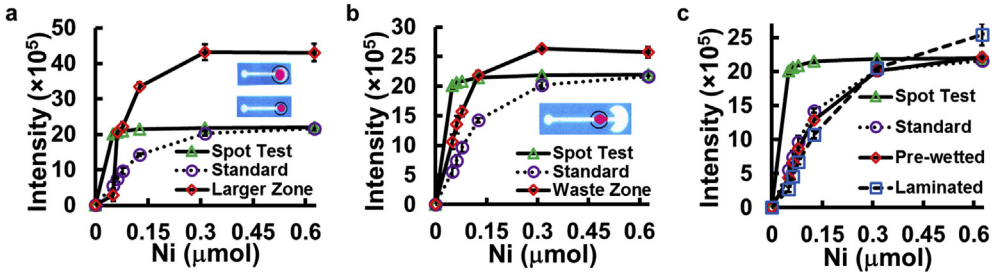


**Fig. 3. a.** Comparison between the standard channel and the larger zone modified test (inset: devices are shown above the legend, with the larger zone device above the standard). **b.** Comparison of standard channel to the waste zone modified device (inset: device is shown above the legend). **c.** Comparison of the standard test versus one that was pre-wetted with Millipore water and the laminated device.

increased to 78% and 28%, respectively (Fig. 4, n = 4). As opposed to what was observed in Section 3.4, the elution step increases both the maximum signal and sensitivity to statistically significant values. (see Table 1)

### 3.11. $Mn(PAR)_2$

To show these concepts were not unique to the Ni(II)-dmg chemistry, Mn(II) was measured with PAR as the colorimetric ligand. Unlike $Ni(dmg)_2$, the $Mn(PAR)_2$ complex does not precipitate under aqueous conditions, which provides for variation in the nature of the colorimetric reaction. A comparison of the results for the standard device and the additive device are shown in Fig. S4. The combination device increased the maximum signal by 94%. The sensitivity was not calculated due to the very high increase in signal at the amounts of Mn(II) used. This test provides more evidence that the additive device is potentially applicable to a variety of different systems.

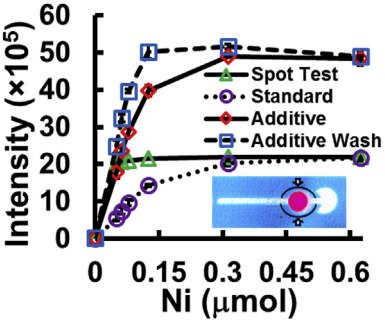


**Fig. 4.** The comparison of the standard test versus the additive test along with its washing (inset: device is shown below legend).

**Table 1**
Tabulated comparison of maximum signal and sensitivity between devices.

| Device | Maximum Signal (Intensity × $10^5$) | Sensitivity (Intensity × $10^5$ μmol$^{-1}$) |
|---|---|---|
| Spot Test | 22.0 ± 0.3 | – |
| Standard | 22.8 ± 0.6 | 115 |
| Laser Cut | 18.5 ± 0.2 | 60.8 |
| Elution Step | 21.2 ± 0.5 | 164 |
| Small Inlet | 21.8 ± 0.3 | 117 |
| Larger Detection Zone | 43.9 ± 1.5 | 285 |
| Waste Zone | 26.4 ± 0.4 | 176 |
| Pre-wetted | 24.6 ± 1.3 | 105 |
| Laminated | 30.6 ± 2.4 | 88 |
| Additive | 49.0 ± 0.2 | 320 |
| Additive + Wash | 51.7 ± 0.6 | 407 |

## 4. Conclusion

As the field of fast and cost-effective sensors grows, it is important to consider simple concepts to lower detection limits and increase dynamic range. The intricate cellulose network commonly used in μPADs provides many torturous avenues for sample retention resulting in poor detection limits and low sensitivity. This study investigated travel distances, wax barriers, shape of both detection and sampling zones, pre-swelling fibers, lamination, waste zones, and washing steps to compare with the standard and spot test devices. By selecting and combining the manipulations that increased performance of the device, we increased both the maximum signal and sensitivity by 78% and 28%, respectively. Significant performance enhancement was also observed when moving to the detection of Mn(II) with PAR suggesting that these improvements may be applied more generally. While this study was aimed at reducing metal sample loss to the μPAD, the retention of various sample types, such as biological analytes, on the device can potentially be reduced by employing these modifications and principles. The significance of this work may also translate to ePAD technology by increasing the concentration of analytes on the surface of the electrodes. For example, in a stripping voltammetry detection scheme, where the detection method relies on efficient sample delivery to the surface of the electrode, these principles may also apply.

## Acknowledgements

The authors would like to thank Dr. Jaclyn Adkins for her useful discussions. Financial support for this work was provided by the National Science Foundation [1534786] and the National Institute of Occupational Health and Safety [R01OH010662]. The authors declare no competing financial interests.

## Appendix A. Supplementary data

Supplementary data related to this article can be found at https://doi.org/10.1016/j.aca.2018.01.036.

## References

[1] C.P. Wild, Complementing the genome with an “exposome”: the outstanding challenge of environmental exposure measurement in molecular epidemiology, Cancer Epidemiol. Biomark. Prev. 14 (2005) 1847–1850.
[2] D.D. Liana, B. Raguse, J.J. Gooding, E. Chow, Recent advances in paper-based sensors, Sensors 12 (2012) 11505.
[3] A.K. Yetisen, M.S. Akram, C.R. Lowe, Paper-based microfluidic point-of-care diagnostic devices, Lab a Chip 13 (2013) 2210–2251.
[4] D.M. Cate, J.A. Adkins, J. Mettakoonpitak, C.S. Henry, Recent developments in paper-based microfluidic devices, Anal. Chem. 87 (2015) 19–41.
[5] J. Adkins, K. Boehle, C. Henry, Electrochemical paper-based microfluidic devices, Electrophoresis 36 (2015) 1811–1824.

[6] Y.Y. Xia, J. Si, Z.Y. Li, Fabrication techniques for microfluidic paper-based analytical devices and their applications for biological testing: a review, Biosens. Bioelectron. 77 (2016) 774–789.
[7] N.A. Meredith, C. Quinn, D.M. Cate, T.H. Reilly, J. Volckens, C.S. Henry, Paper-based analytical devices for environmental analysis, Analyst 141 (2016) 1874–1887.
[8] L. Busa, S. Mohammadi, M. Maeki, A. Ishida, H. Tani, M. Tokeshi, Advances in microfluidic paper-based analytical devices for food and water analysis, Micromachines 7 (2016) 86.
[9] Y. Lin, D. Gritsenko, S. Feng, Y.C. Teh, X. Lu, J. Xu, Detection of heavy metal by paper-based microfluidics, Biosens. Bioelectron. 83 (2016) 256–266.
[10] W. Dungchai, O. Chailapakul, C.S. Henry, Electrochemical detection for paper-based microfluidics, Anal. Chem. 81 (2009) 5821–5826.
[11] P. Kauffman, E. Fu, B. Lutz, P. Yager, Visualization and measurement of flow in two-dimensional paper networks, Lab a Chip 10 (2010) 2614–2617.
[12] E. Fu, S.A. Ramsey, P. Kauffman, B. Lutz, P. Yager, Transport in two-dimensional paper networks, Microfluid. Nanofluidics 10 (2011) 29–35.
[13] J. Kim, H.-Y. Kim, On the dynamics of capillary imbibition, J. Mech. Sci. Technol. 26 (2012) 3795–3801.
[14] X. Li, D.R. Ballerini, W. Shen, A perspective on paper-based microfluidics: current status and future trends, Biomicrofluidics 6 (2012), 011301–011301-011313.
[15] Y. Xu, T. Enomae, Paper substrate modification for rapid capillary flow in microfluidic paper-based analytical devices, RSC Adv. 4 (2014) 12867–12872.
[16] J. Songok, M. Toivakka, Controlling capillary-driven surface flow on a paper-based microfluidic channel, Microfluid. Nanofluidics 20 (2016) 9.
[17] J. Houghtaling, T. Liang, G. Thiessen, E. Fu, Dissolvable bridges for manipulating fluid volumes in paper networks, Anal. Chem. 85 (2013) 11201–11204.
[18] S. Jahanshahi-Anbuhi, P. Chavan, C. Sicard, V. Leung, S.M.Z. Hossain, R. Pelton, J.D. Brennan, C.D.M. Filipe, Creating fast flow channels in paper fluidic devices to control timing of sequential reactions, Lab a Chip 12 (2012) 5079–5085.
[19] E. Elizalde, R. Urteaga, C.L.A. Berli, Rational design of capillary-driven flows for paper-based microfluidics, Lab a Chip 15 (2015) 2173–2180.
[20] E. Evans, E.F.M. Gabriel, W.K.T. Coltro, C.D. Garcia, Rational selection of substrates to improve color intensity and uniformity on microfluidic paper-based analytical devices, Analyst 139 (2014) 2127–2132.
[21] E. Booth, J.D.H. Strickland, The compounds formed between nickel(II) and dimethylglyoxime by alkaline oxidation, J. Am. Chem. Soc. 75 (1953) 3017–3019.
[22] M.M. Mentele, J. Cunningham, K. Koehler, J. Volckens, C.S. Henry, Microfluidic paper-based analytical device for particulate metals, Anal. Chem. 84 (2012) 4474–4480.
[23] E. Carrilho, A.W. Martinez, G.M. Whitesides, Understanding wax printing: a simple micropatterning process for paper-based microfluidics, Anal. Chem. 81 (2009) 7091–7095.
[24] S. Hong, W. Kim, Dynamics of water imbibition through paper channels with wax boundaries, Microfluid. Nanofluidics 19 (2015) 845–853.
[25] D. Zhou, L. Zhang, J. Zhou, S. Guo, Cellulose/chitin beads for adsorption of heavy metals in aqueous solution, Water Res. 38 (2004) 2643–2650.
[26] M. d'Halluin, J. Rull-Barrull, G. Bretel, C. Labrugère, E. Le Grognec, F.-X. Felpin, Chemically modified cellulose filter paper for heavy metal remediation in water, ACS Sustain. Chem. Eng. 5 (2) (2017) 1965–1973.
[27] S. Mohammadi, L.S.A. Busa, M. Maeki, R.M. Mohamadi, A. Ishida, H. Tani, M. Tokeshi, Novel concept of washing for microfluidic paper-based analytical devices based on capillary force of paper substrates, Anal. Bioanal. Chem. 408 (2016) 7559–7563.
[28] S. Mendez, E.M. Fenton, G.R. Gallegos, D.N. Petsev, S.S. Sibbett, H.A. Stone, Y. Zhang, G.P. López, Imbibition in porous membranes of complex shape: quasi-stationary flow in thin rectangular segments, Langmuir 26 (2010) 1380–1385.
[29] J.A. Adkins, E. Noviana, C.S. Henry, Development of a quasi-steady flow electrochemical paper-based analytical device, Anal. Chem. 88 (2016) 10639–10647.
[30] O.A. El Seoud, L.C. Fidale, N. Ruiz, M.L.O. D'Almeida, E. Frollini, Cellulose swelling by protic solvents: which properties of the biopolymer and the solvent matter? Cellulose 15 (2008) 371–392.
[31] D. Klemm, B. Philipp, T. Heinze, U. Heinze, W. Wagenknecht, General Considerations on Structure and Reactivity of Cellulose: Section 2.2–2.2.3, Comprehensive Cellulose Chemistry, Wiley-VCH Verlag GmbH & Co. KGaA2004, pp. 43–82.
[32] D. Klemm, B. Philipp, T. Heinze, U. Heinze, W. Wagenknecht, General Considerations on Structure and Reactivity of Cellulose: Section 2.3–2.3.7, Comprehensive Cellulose Chemistry, Wiley-VCH Verlag GmbH & Co. KGaA2004, pp. 83–129.
[33] L.C. Fidale, N. Ruiz, T. Heinze, O.A.E. Seoud, Cellulose swelling by aprotic and protic solvents: what are the similarities and differences? Macromol. Chem. Phys. 209 (2008) 1240–1254.